

Transistors performance in the sub-1 nm technology node based on one-dimensional nanomaterials

Jingtian Fang*, William G. Vandenberghe, and Massimo V. Fischetti

Department of Materials Science and Engineering, The University of Texas at Dallas, USA

*Email: jingtian.fang@utdallas.edu

Abstract—An open boundary-conditions full-band quantum transport formalism with a plane-wave basis based on empirical pseudopotentials is used to self-consistently simulate transistors in the sub-1 nm technology node, with one-dimensional silicon nanowires, armchair-edge graphene nanoribbons, and zigzag-edge carbon nanotubes as the channel. The electrostatic potential energy and charge density distribution are shown. Current-voltage characteristics of these devices are obtained.

I. INTRODUCTION

For the upcoming ultrascaled CMOS field-effect transistors (FETs), the characterizing dimension of the channel, such as the body size of the materials W_{body} , the effective oxide thickness (EOT), and the physical gate length L_g , decreases significantly comparing to the current stage of the technology development [1]. Due to quantum confinement effects, the materials in a smaller dimension show different energy band structure and band gap in contrast with the bulk form of the materials, which can then affect the transport properties of transistors made out of them. Another feature in the revolutionary device design is using an efficient gating structure, such as a geometrically fin-shape [2], [3] or a gate-all-around (GAA) structure [4], [5], to enable stronger electrostatic control in the gate region [6] and overcome the short-channel effects (SCEs) and the drain-induced barrier-lowering (DIBL) effect. In this paper, we present a state-of-the-art theoretical simulation of quantum transport in GAAFETs using 1D nanomaterials armchair-edge graphene nanoribbons (aGNRs) [7], carbon nanotubes (CNTs) [8], [9], and silicon nanowires (SiNWs) as the channel. Current-voltage characteristics of FETs using these different materials are presented and discussed. An in-house three-dimensional Schrödinger/Poisson simulator is applied to perform the simulations self-consistently.

II. THEORY

When simulating electron transport in semiconducting devices, the open boundary-conditions plane-wave full-band quantum transport formalism [10]–[12] is applied using the envelope-wavefunction approximation to deal with the slowly changing external potential along the electron transport direction z . Essentially, linear systems of the form

$$(\mathbf{H} - E\mathbf{I} + \Sigma_L + \Sigma_R)\phi = [\mathbf{RHS}]_L^{\text{inj}} + [\mathbf{RHS}]_R^{\text{inj}} \quad (1)$$

are solved to obtain the envelop wavefunctions for different drain-source bias V_{DS} and gate-source bias V_{GS} . In Eq. (1), \mathbf{H} is the Hamiltonian for the closed system using empirical

pseudopotentials which incorporates the lattice potential and the external potential effect, E is the injection energy of electrons, \mathbf{I} is the identity matrix, Σ_L and Σ_R are the self-energies of the contacts which represent the termination of the device with the source and drain reservoirs using the open-boundary conditions, ϕ is the envelope wavefunction in the reciprocal space which in each z is composed of the number of plane-wave basis N_G , $\phi_E(z) = [\phi_{G_1}(z) \phi_{G_2}(z) \cdots \phi_{G_{N_G}}(z)]^T$, and $[\mathbf{RHS}]_L^{\text{inj}}$ and $[\mathbf{RHS}]_R^{\text{inj}}$ are the terms representing the amplitudes of the waves injected from the contacts.

To calculate the charge density, we perform at first a 3D Fourier transform of $\phi_E(z)$ at each z for each injection energy $E = E(k_z)$ to obtain the wavefunctions $\psi_E(z, \mathbf{r}_{||})$ in the real space and then average the square of the real-space wavefunction $|\psi_E(z, \mathbf{r}_{||})|^2$ over z in one unit cell. With the average $|\psi_E(z, \mathbf{r}_{||})|^2$ in all z forming the 3D wavefunctions $|\psi_E(\mathbf{r})|^2$, the charge density is calculated as

$$n(\mathbf{r}) = \frac{1}{\pi} \sum_{\nu=L,R} \int_{1\text{stBZ}} |\psi_E(\mathbf{r})|^2 F(E, E_F^\nu) dk_z, \quad (2)$$

since we account for electron injection from the left ($\nu = L$) and right ($\nu = R$) contacts and the occupation of the injection energy state is determined by the Fermi-Dirac distribution function $F(E, E_F^\nu)$, with respect to the Fermi level in the contacts E_F^ν .

In order to do a self-consistent calculation, we need to update the external potential $V(\mathbf{r})$ by solving the three-dimensional Poisson's equation

$$\nabla^2 V(\mathbf{r}) = - \frac{e(N_D(\mathbf{r}) - n(\mathbf{r}) - N_A(\mathbf{r}) + p(\mathbf{r}))}{\epsilon} \quad (3)$$

with $n(\mathbf{r})$ calculated in Eq. (2) until the convergence is satisfied with some criterion. In Eq. (3), $N_D(\mathbf{r})$ is the donor density, $N_A(\mathbf{r})$ is the acceptor density in the device, $p(\mathbf{r})$ is the hole density calculated similar to $n(\mathbf{r})$, and ϵ is the dielectric constant. The self-consistent scheme for solving the Schrödinger and Poisson's equations is illustrated in Fig. 1.

After convergence is obtained, the current density is evaluated using

$$j(z) = \frac{i\hbar}{2m} \sum_G (\phi_G(z))^* \left(\frac{d\phi_G(z)}{dz} + iG_z \phi_G(z) \right) \quad (4)$$

and the device current is estimated with the Fermi-Dirac distribution as well.

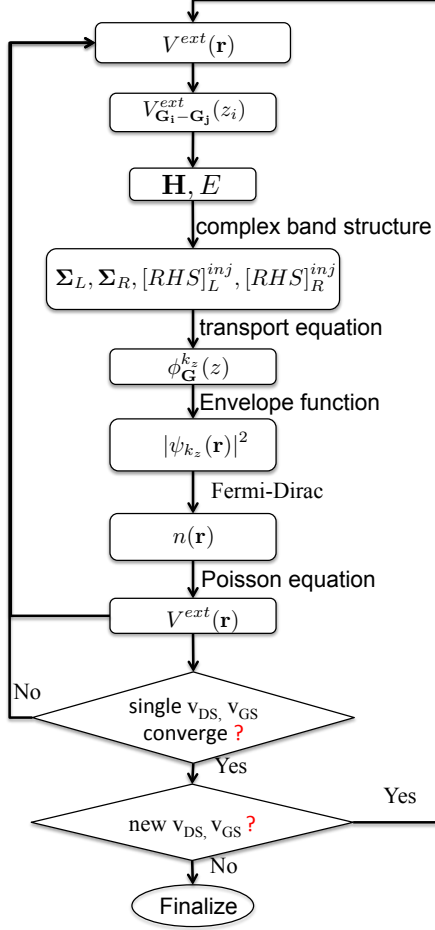


Figure 1: Flow chart for solving the one-dimensional full-band plane-wave quantum transport Schrödinger equation and the three-dimensional Poisson's equation self-consistently.

III. RESULTS

A. Silicon nanowire FETs

For SiNWFETs, we choose a device length $L = 21.72$ nm, a $L_g = 6.52$ nm, and an EOT = 0.43 nm. Figure 2a shows a wire which has three atomic layers on the sides and we define it as a (3×3) -SiNW. The cross-sectional body size is determined by the side length which measures 0.34 nm. Figure 2b shows the size dependence of the band gap for $[001]$ -oriented SiNWs with square-shape cross-sections.

For simulating this device and following devices, the donor density in the source and drain contact is set as $1 \times 10^8 m^{-3}$ and the acceptor density in the gate is set as $1 \times 10^8 m^{-3}$ as well. The charge density and potential energy distributions after the self-consistent calculation at the simulated bias are shown respectively in Figs. 3 and 4 one-dimensionally along z , after averaging the three-dimensional distribution of them in the cross-section of each z . The current determined after the self-consistency for all the applied biases is shown in

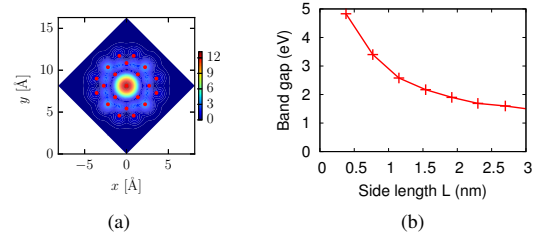


Figure 2: (a) Cross-sectional view of a $[001]$ -oriented (3×3) -SiNW, with the silicon body passivated by hydrogen and surrounded by vacuum. Atoms are indicated by red dots superimposed on a contour plot of $|\psi(z, \mathbf{r}_{\parallel})|^2$ for z located in the contact without the effect of external potential $V(\mathbf{r})$. (b) Body-size dependence of the band gap for square cross-section SiNWs oriented in the $[001]$ direction.

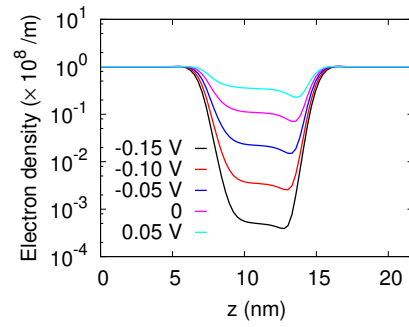


Figure 3: Self-consistent electron density distribution of a $[001]$ -oriented (3×3) -SiNWFET when applying the same drain-source bias $V_{DS} = 0.1$ V and different gate-source bias V_{GS} . Charge neutrality can be observed in the extended source/device contact and drain/device contact. A high V_{GS} stops carrier flow from the source to the drain in the device.

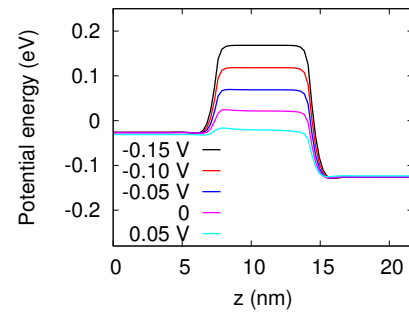


Figure 4: Self-consistent electrostatic potential energy profile of the (3×3) -SiNWFET when applying the same $V_{DS} = 0.1$ V and the V_{GS} ranging from -0.15 V to 0.05 V.

Fig. 5. An excellent subthreshold slope (SS) of 76 mV/decade is achieved for this device.

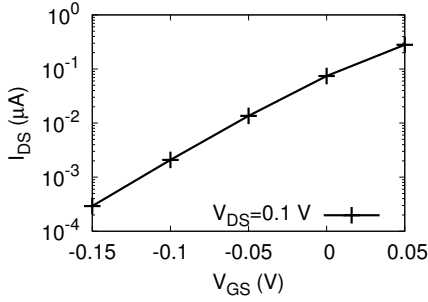


Figure 5: I_{DS} - V_{GS} characteristics of the (3×3) -SiNWFET at $V_{DS} = 0.1$ V. This device shows a subthreshold swing (SS) of 76 mV/decade.

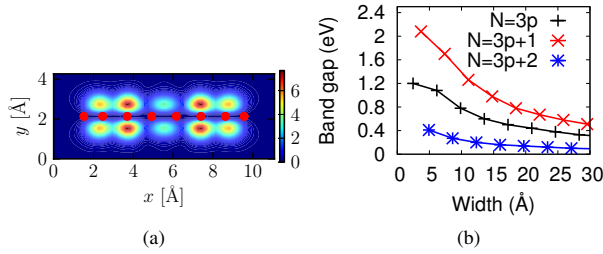


Figure 6: (a) Cross-sectional view of a 6-aGNR terminated by hydrogen. Atoms are indicated by red dots superimposed on a contour plot of $|\psi(z, r_{\parallel})|^2$. (b) Ribbon-width dependence of the band gap for aGNRs.

B. Armchair-edge GNRFETs

For aGNRFETs, the device length is chosen as $L=17.06$ nm, the gate length is $L_g=5.12$ nm, and the EOT=0.43 nm. Figure 6a shows a 6-aGNR model with six carbon dimer lines in the center and the hydrogen termination on both edges. The body size is characterized with its width 0.62 nm. Fig. 6b shows the width dependence of the band gap.

The charge density and potential energy profiles are shown in Figs. 7 and 8, respectively. Since the 3-aGNR has a smaller effective mass than the (3×3) -SiNW, when the electron collides elastically with the potential barrier, it reflects further away from the gate contact for the 3-aGNR than for the SiNW and more carriers accumulate in the region close to the gate which introduces the tiny bump in Fig. 7 and the quantum wells in Fig. 8, whereas it is flat in this region in Figs. 3 and 4. The device characteristics of the 3-aGNRFET are shown in Fig. 9. A poor SS of ~ 120 mV/decade is observed.

C. Zigzag CNTFETs

The model and the diameter dependence of the band gap of zCNTs are shown in Figs. 10a and 10b, from which we observe that the smallest semiconducting tube is the $(10,0)$ -zCNT owning a diameter $D = 0.78$ nm and a band gap $E_g = 0.22$ eV. This diameter results in smaller reciprocal-space translation

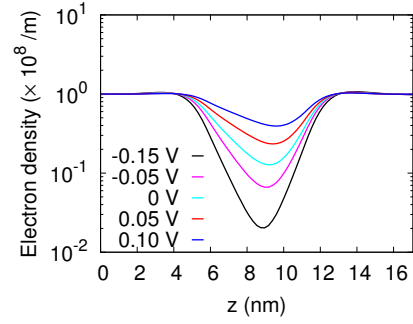


Figure 7: Self-consistent electron density distribution of a 3-aGNRFET with $V_{DS} = 0.1$ V and different V_{GS} ranging from -0.15 to 0.10 V. Charge neutrality is satisfied in the extended source and drain contact region. And in the region close to the gate contact, the electron density is higher than the doping density, unlike the neutrality observed for the (3×3) -SiNWFET.

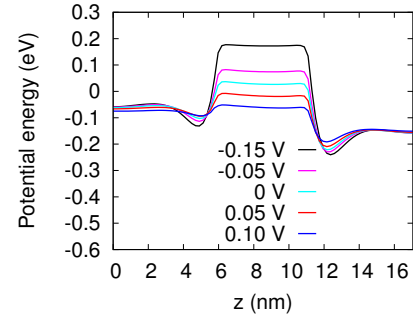


Figure 8: Self-consistent potential energy distribution of the 3-aGNRFET applied with $V_{DS} = 0.1$ V and different V_{GS} . This device shows quantum wells in the region close to the gate, which is different from the (3×3) -SiNWFET.

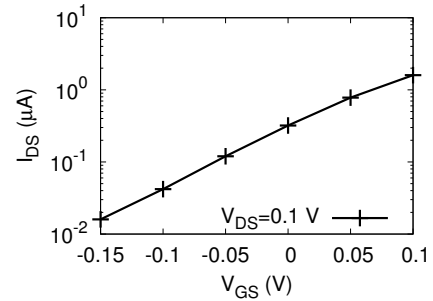


Figure 9: I_{DS} - V_{GS} characteristics of the 3-aGNRFET at $V_{DS} = 0.1$ V. This device shows a SS of ~ 120 mV/dec.

vectors and a larger number of the plane-wave basis N_G when using the same E_{cutoff} as what's used for aGNR. Currently, a $(10,0)$ -zCNTFET is simulated with a shorter device length $L=8.52$ nm, a shorter gate length $L_g=2.13$ nm, an EOT=0.43

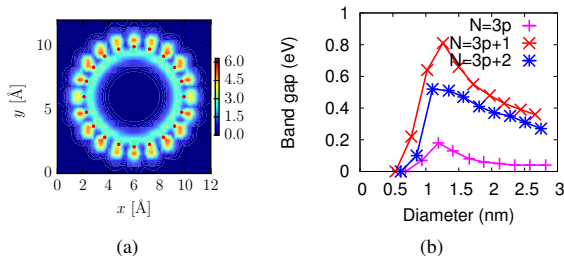


Figure 10: (a) Cross-sectional view of a (10,0)-zCNT. A contour plot of $|\psi(z, r_{||})|^2$ in the cross section is shown. (b) Diameter dependence of the band gap for zCNTs.

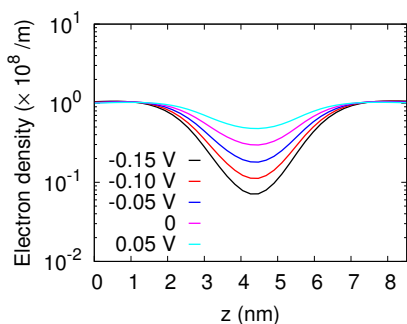


Figure 11: Self-consistent electron density distribution of a (10,0)-zCNTFET with $V_{DS} = 0.1$ V and different V_{GS} applied.

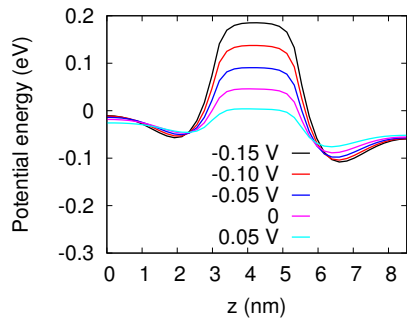


Figure 12: Self-consistent potential energy distribution of the (10,0)-zCNTFET with $V_{DS} = 0.1$ V and different V_{GS} . This device shows quantum wells in the region close to the gate similar to the 3-aGNRFET since it also has a smaller effective mass compared to SiNWs.

nm, and a $E_{\text{cutoff}}=10$ Ry to decrease the matrix size so that the simulation can be implemented in a shorter running time. The preliminary results show the charge density and potential energy distribution in Figs. 11 and 12, respectively. We find that the zCNTFET shows the same features as the aGNRFET.

The transport properties of the device are shown in Fig. 13 from which a $SS \sim 190$ mV/dec is extracted.

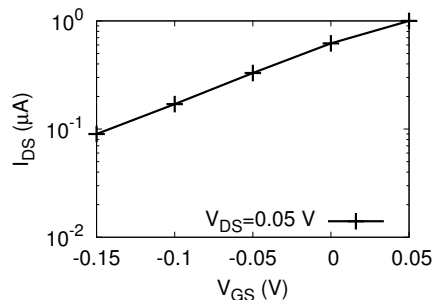


Figure 13: I_{DS} - V_{GS} characteristics of the (10,0)-zCNTFET with $V_{DS} = 0.05$ V. This device shows a SS of ~ 190 mV/dec.

IV. CONCLUSIONS

Gate-all-around transistors in the sub-1 nm technology node using three kinds of 1D nanomaterials in the channel are simulated. The ballistic performance is obtained with their electrical properties shown. Silicon nanowires show the best feature in terms of the subthreshold swing.

REFERENCES

- [1] International Technology Roadmap for Semiconductor, "Process integration, devices, and structures," [Online], 2013.
- [2] F.-L. Yang, D.-H. Lee, H.-Y. Chen, C.-Y. Chang, S.-D. Liu, C.-C. Huang, T.-X. Chung, H.-W. Chen, C.-C. Huang, Y.-H. Liu *et al.*, "5nm-gate nanowire finfet," in *VLSI Technology, 2004. Digest of Technical Papers. 2004 Symposium on.* IEEE, 2004, pp. 196–197.
- [3] E. Yu, L. Chang, S. Ahmed, H. Wang, S. Bell, C.-Y. Yang, C. Tabery, C. Ho, Q. Xiang, T.-J. King *et al.*, "Finfet scaling to 10 nm gate length," in *Electron Devices Meeting, 2002. IEDM'02. International.* IEEE, 2002, pp. 251–254.
- [4] J. Gu, Y. Liu, Y. Wu, R. Colby, R. G. Gordon, and P. D. Ye, "First experimental demonstration of gate-all-around iii-v mosfets by top-down approach," in *Electron Devices Meeting (IEDM), 2011 IEEE International.* IEEE, 2011, pp. 33–2.
- [5] X. Chen and C. M. Tan, "Modeling and analysis of gate-all-around silicon nanowire {FET}," *Microelectronics Reliability*, vol. 54, no. 67, pp. 1103 – 1108, 2014. [Online]. Available: <http://www.sciencedirect.com/science/article/pii/S0026271413004472>
- [6] M. V. Fischetti, B. Fu, and W. G. Vandenberghe, "Theoretical study of the gate leakage current in sub-10-nm field-effect transistors," *Electron Devices, IEEE Transactions on*, vol. 60, no. 11, pp. 3862–3869, 2013.
- [7] X. Li, X. Wang, L. Zhang, S. Lee, and H. Dai, "Chemically derived, ultrasmooth graphene nanoribbon semiconductors," *Science*, vol. 319, no. 5867, pp. 1229–1232, 2008.
- [8] A. Javey, J. Guo, Q. Wang, M. Lundstrom, and H. Dai, "Ballistic carbon nanotube field-effect transistors," *nature*, vol. 424, no. 6949, pp. 654–657, 2003.
- [9] A. D. Franklin, M. Luisier, S.-J. Han, G. Tulevski, C. M. Breslin, L. Gignac, M. S. Lundstrom, and W. Haensch, "Sub-10 nm carbon nanotube transistor," *Nano letters*, vol. 12, no. 2, pp. 758–762, 2012.
- [10] B. Fu, "Quantum transport: from effective mass approximation to full band," Ph.D. dissertation, The University of Texas at Dallas, Richardson, TX, 2013.
- [11] J. Fang, W. G. Vandenberghe, and M. V. Fischetti, "Full-band ballistic quantum transport in nanostructures using empirical pseudopotential," in *Computational Electronics (IWCE), 2014 International Workshop on.* IEEE, 2014, pp. 1–3.
- [12] J. Fang, W. G. Vandenberghe, and M. V. Fischetti, "Theoretical prediction of ballistic performance of sub-1 nm transistors using full-band plane-wave quantum transport simulations," [unpublished], 2015.